Codella Roberto (Orcid ID: 0000-0003-1608-1899)

Overexpression of UCP3 decreases mitochondrial efficiency in mouse skeletal muscle *in vivo*

Roberto Codella[1,2,3], Tiago C. Alves[1], Douglas E. Befroy[1,4], Cheol Soo Choi[1], Livio Luzi[2,3], Douglas L. Rothman[4], Richard G. Kibbey[1], Gerald I. Shulman[1]

[1] Departments of Internal Medicine and Cellular & Molecular Physiology, Yale School of Medicine, New Haven, CT, USA

[2] Department of Biomedical Sciences for Health, Università degli Studi di Milano, Milan, Italy

[3] Department of Endocrinology, Nutrition and Metabolic Diseases, IRCCS MultiMedica, Milan, Italy

[4] Department of Diagnostic Radiology, Yale School of Medicine, New Haven, CT, USA

Running head title: *In-vivo mitochondrial efficiency in UCP3^{+} mice*

Corresponding author

Gerald I. Shulman, MD, PhD

Departments of Internal Medicine and Cellular and Molecular Physiology

Yale School of Medicine

333 Cedar Street, New Haven – CT 06520-8020, USA (TAC S269, PO Box 208020)

Phone: +1-203-785-5447

Fax: +1-203-737-4059

E-mail: gerald.shulman@yale.edu

This article has been accepted for publication and undergone full peer review but has not been through the copyediting, typesetting, pagination and proofreading process which may lead to differences between this version and the Version of Record. Please cite this article as doi: 10.1002/1873-3468.14494

Codella Roberto (Orcid ID: 0000-0003-1608-1899)

Abbreviations

AFP	Adiabatic Full Passage
AHP	Adiabatic Half Passage
APE	Atom Percent Excess
FAO	Fatty Acid Oxidation
FID	Free Induction Decay
FT	Fourier Transformation
GDP	Guanosine diphosphate
IMM	Inner Mitochondrial Membrane
KO	Knock-Out, mice with inactivated ("knocked out") gene/s
MRS	Magnetic Resonance Spectroscopy
NMR	Nuclear Magnetic Resonance
POCE	Proton-Observe Carbon-Edited
PPA	Phenylphosphonic acid
RC	Regular Chow
ROS	Reactive Oxygen Species
TCAI	Tricarboxylic Acid Cycle intermediates
TG	Transgenic
T_R	Repetition Time
UCP3	Uncoupling Protein-3
V_{ATP}	$Pi \rightarrow ATP$ flux
V_{TCA}	Tricarboxylic Acid Cycle flux

WT Wild Type

Abstract

Uncoupling protein-3 (UCP3) is a mitochondrial transmembrane protein highly expressed in muscle that has been implicated in regulating the efficiency of mitochondrial oxidative phosphorylation. Increasing UCP3 expression in skeletal muscle enhances proton leak across the inner mitochondrial membrane and increases oxygen consumption in isolated mitochondria, but its precise function *in vivo* has yet to be fully elucidated. To examine whether muscle-specific overexpression of UCP3 modulates muscle mitochondrial oxidation *in vivo*, rates of ATP synthesis were assessed by ^{31}P magnetic resonance spectroscopy (MRS) and rates of mitochondrial oxidative metabolism were measured by assessing the rate of [2-^{13}C]acetate incorporation into muscle [4-^{13}C]- , [3-^{13}C]-glutamate and [4-^{13}C]-glutamine by high resolution ^{13}C/^{1}H MRS. Using this approach we found that overexpression of UCP3 in skeletal muscle was accompanied by increased muscle mitochondrial inefficiency *in vivo* as reflected by a 42% reduction in the ratio of ATP synthesis to mitochondrial oxidation.

Keywords: muscle energy metabolism, magnetic resonance spectroscopy, mitochondrial efficiency, mitochondrial uncoupling

Introduction

Uncoupling protein-3 (UCP3) is a member of the mitochondrial carrier protein superfamily predominantly expressed in skeletal muscle and localized to the inner mitochondrial membrane (IMM)[1]. Although discovered in 1997, the biochemical and physiological functions of UCP3 remain unclear [2,3]. UCP3 was initially thought to be involved in non-shivering thermogenesis because of its high degree of homology to UCP1[4,5]. However, UCP3 is expressed at a very low level in brown adipose tissue compared to UCP1 and its putative role in thermogenesis remains a matter of debate. UCP3 activity may contribute to an array of metabolic disorders ranging from type 2 diabetes [6] to mitochondrial dysfunction and aging [7,8]. Almost two decades ago Gong et al. showed that UCP3 overexpression lowered the proton gradient across the (IMM) [5] indicating that it may modulate mitochondrial oxidative phosphorylation. In support of this interpretation, mitochondria isolated from skeletal muscle of mice overexpressing UCP3 had increased state 4 of respiration, i.e. increased proton leak across the IMM [9]. Similarly, skeletal muscle mitochondria in mice lacking UCP3 (UCP3-KO) exhibited decreased state 4 respiration and decreased concentrations of ADP, a key regulator of ATP production [10]. Furthermore, the ratio of $P_i \rightarrow$ ATP flux / TCA cycle activity determined in the hindlimb muscles of these UCP3-KO mice was found to be 2-4-fold higher than in wild-type (WT) mice, suggesting that UCP3 may also uncouple mitochondrial oxidative phosphorylation *in vivo* [11]. However, conflicting results from other studies [12] raise the question of whether this protein possesses an uncoupling activity that is physiologically relevant [13]. The majority of efforts to define the function of UCP3 have been conducted in isolated mitochondria [14]; in this study we sought to examine its role *in vivo* by exploiting non-invasive magnetic resonance spectroscopy (MRS) techniques. We performed an *in situ* infusion of [2-^{13}C]-acetate combined with *ex vivo* MRS analysis of muscle biopsies to determine rates of substrate oxidation via the tricarboxylic acid cycle (V_{TCA}) and utilized *in vivo* ^{31}P saturation transfer MRS to assess the unidirectional $P_i \rightarrow$ ATP flux (V_{ATP}) [15]. V_{ATP}/V_{TCA} represents an index of the efficiency of mitochondrial oxidative

phosphorylation and we determined whether this was modulated by the overexpression of UCP3 in transgenic mice.

Material and Methods

Animals

Details concerning the generation of mice overexpressing human UCP3 in skeletal muscle have been described previously [11]. Homozygous male transgenic mice showed 2-to-3-fold higher UCP3 protein content (UCP3-TG) in skeletal muscle than wild-type C57BL/6J controls (WT) [16]. Mice were fed regular chow (14% of calories from fat, 60% from carbohydrate, 26% from protein; Prolab RMH 3000; Purina Mills Inc.) *ad libitum*. They were housed under controlled temperature (23 °C) and lighting (12-hour light / 12-hour dark) with free access to water at NIH-Yale Mouse Metabolic Phenotyping Center. Mice were studied at 15-16 weeks old.

Basal metabolic studies

Fat and lean body masses (expressed as percentages of total body mass) in UCP3-TG and WT mice were assessed by ^{1}H-NMR using a Minispec system (Bruker BioSpin, Billerica, MA, USA). A comprehensive animal metabolic monitoring system (CLAMS; Columbus Instruments, Columbus, OH, USA) was also used to evaluate activity, food consumption, and energy expenditure for 10 days.

In vivo skeletal muscle TCA cycle flux (V_{TCA})

Substrate oxidation via the TCA cycle was assessed using a biopsy-based technique. Mice were infused with exogenous ^{13}C-labelled acetate ([2-^{13}C]), TCA cycle flux in muscle was estimated by metabolic modelling of the rate of enrichment of tissue glutamate determined by high-resolution ^{13}C-NMR of an extract of the muscle biopsy.

General procedure: Mice were implanted with a jugular vein catheter 8-10 days before the experimental procedure. After an overnight fast, mice were placed on a plexiglass platform in prone position and anesthetized with ~1% isoflurane in a 20:80 O_2:air mixture via a nose-cone. Physiological parameters (body temperature, ECG, respiration rate,) were monitored continuously to ensure an appropriate depth of anesthesia. Following a 60 min equilibration period, each mouse received a constant infusion of [2-^{13}C]-acetate (10.2 g μg/g/min) and

was sacrificed at specific time points for tissue collection. Plasma samples were obtained by tail-tip bleeds at t = -30, 1, 3, 5, 9, 15, 20, 30, 45, 60 and 90 min after the beginning of the infusion. Plasma acetate concentration and ^{13}C-enrichment were determined by GC-MS [17]. The skeletal muscle complex (soleus-gastrocnemius-tibialis anterior) was obtained at different intervals (0, 2, 4, 6.5, 10, 16, 30, 45, 65, 90 min) during the infusion from each alive, anesthetized, mouse. An average of 6 distinct hindlimbs per each data point (one hindlimb = one mouse) were used to generate complete timecourses of [2-^{13}C]-acetate. Muscles were collected and freeze-clamped in 8 seconds (maximum), *in situ* (Fig. 1A) and then stored in -80 °C refrigerator for further analysis.

Metabolite extraction Muscle extracts for high-field NMR analysis were created using a perchloric acid-based extraction procedure as described previously [11]. The lyophilized supernatant was re-suspended in 500 µl of 50 mM KH_2PO_4 buffer (pH 7.1, 50% D_2O) containing 10mM formate as an internal standard.

POCE-analysis of ^{13}C-enrichments Muscle glutamate and glutamine concentrations and ^{13}C-enrichments were determined by high-resolution Proton-Observe Carbon-Edited (POCE) NMR on a 500MHz Bruker AVANCE system (Bruker Biospin, Billerica, MA, USA). The POCE technique acquires paired ^{1}H spectra: an initial spectrum detects signal from all metabolite protons present in the sample (Supplemental Figure 1A), and in the second spectrum the signal of protons bound to ^{13}C is selectively inverted or 'edited'. The difference in signal between the two spectra corresponds to protons bound to ^{13}C only (Supplemental Figure 1B). Metabolite concentrations can be determined from the initial ^{1}H spectrum with reference to the internal standard. Isotopic ^{13}C-enrichments are calculated from the ratio of the appropriate metabolite signal in the difference spectrum versus the initial spectrum. A full description of this MR method can be found in the book by de Graaf [18]; detailed acquisition conditions have been described previously [19].

Metabolic Modelling Analysis Time courses of muscle [4-^{13}C]- and [3-^{13}C]-glutamate and [4-^{13}C]-glutamine were fitted to a metabolic model of the TCA cycle, as depicted in Fig. 1B. The model describes the flow of ^{13}C-label from plasma [2-^{13}C]-acetate (input function) to glutamate and glutamine (target functions) through two consecutive turns of the TCA cycle. The model also incorporates plasma acetate concentrations and tissue concentrations of glutamate, glutamine and acetate determined experimentally, as described above. The TCA cycle intermediates (TCAI) citrate, α-ketoglutarate (αKG), oxaloacetate (OAA) and acetyl-CoA were below the

threshold of detection using these NMR methods. However, the individual content of the TCAI is extremely low and each was therefore assigned a concentration of 0.05 μmol·g^{-1}. Collectively, a small pool approximation with respect glutamate and glutamine can be assumed and the assigned concentrations therefore have no impact on the modelled rates. The set of differential equations that fully characterize this metabolic scheme are shown below. Metabolic modelling to establish V_{TCA} and other rates of substrate utilization was performed using CWave software (version 3.5.5) [20], running in MatLab (R2016b).

Metabolic modelling of the TCA cycle in skeletal muscle (Figure 1B). Differential equations describing the flow of ^{13}C label

$$\frac{d\,[2-{}^{13}C]AcetylCoA}{dt} = V_{AC}\frac{[2-{}^{13}C]Acetate}{Acetate} + V_{Dil} - V_{TCA}\frac{[2-{}^{13}C]AcetylCoA}{AcetylCoA}$$

$$\frac{d\,[4-{}^{13}C]Citrate}{dt} = V_{TCA}\frac{[2-{}^{13}C]AcetylCoA}{AcetylCoA} - V_{TCA}\frac{[4-{}^{13}C]Citrate}{Citrate}$$

$$\frac{d\,[4-{}^{13}C]\alpha KG}{dt} = V_{TCA}\frac{[4-{}^{13}C]Citrate}{Citrate} + V_X\frac{[4-{}^{13}C]Glutamate}{Glutamate} - (V_{TCA}+V_X)\frac{[4-{}^{13}C]\alpha KG}{\alpha KG}$$

$$\frac{d\,[4-{}^{13}C]Glutamate}{dt} = V_X\frac{[4-{}^{13}C]\alpha KG}{\alpha KG} + V_{GS}\frac{[4-{}^{13}C]Glutamine}{Glutamine} - (V_X+V_{GS})\frac{[4-{}^{13}C]Glutamate}{Glutamate}$$

$$\frac{d\,[3-{}^{13}C]OAA}{dt} = 0.5V_{TCA}\frac{[4-{}^{13}C]\alpha KG}{\alpha KG} + 0.5V_{TCA}\frac{[3-{}^{13}C]\alpha KG}{\alpha KG} - V_{TCA}\frac{[3-{}^{13}C]OAA}{OAA}$$

$$\frac{d\,[3-{}^{13}C]Citrate}{dt} = V_{TCA}\frac{[3-{}^{13}C]OAA}{OAA} - V_{TCA}\frac{[3-{}^{13}C]Citrate}{Citrate}$$

$$\frac{d\,[3-{}^{13}C]\alpha KG}{dt} = V_{TCA}\frac{[3-{}^{13}C]Citrate}{Citrate} + V_X\frac{[3-{}^{13}C]Glutamate}{Glutamate} - (V_{TCA}+V_X)\frac{[3-{}^{13}C]\alpha KG}{\alpha KG}$$

$$\frac{d\,[3-{}^{13}C]Glutamate}{dt} = V_X\frac{[3-{}^{13}C]\alpha KG}{\alpha KG} + V_{GS}\frac{[3-{}^{13}C]Glutamine}{Glutamine} - (V_X+V_{GS})\frac{[3-{}^{13}C]Glutamate}{Glutamate}$$

$$\frac{d\,[4-{}^{13}C]Glutamine}{dt} = V_{GS}\frac{[4-{}^{13}C]Glutamate}{Glutamate} + V_{Dil-Gln} - (V_{GS}+V_{Exit-Gln})\frac{[4-{}^{13}C]Glutamine}{Glutamate}$$

$$\frac{d\,[3-{}^{13}C]Glutamine}{dt} = V_{GS}\frac{[3-{}^{13}C]Glutamate}{Glutamate} + V_{Dil-Gln} - (V_{GS}+V_{Exit-Gln})\frac{[3-{}^{13}C]Glutamine}{Glutamate}$$

Mass Balance equations

$$V_{TCA} = V_{Dil} + V_{AC}$$

$$V_{Dil-Gln} = V_{Exit-Gln}$$

<u>In vivo skeletal muscle $P_i \rightarrow ATP$ flux (V_{ATP})</u>

^{31}P saturation-transfer MRS experiments were performed to measure the rate of phosphate transfer between inorganic phosphate (P_i) and ATP ($P_i \rightarrow$ ATP flux, V_{ATP}) in skeletal muscle [15]. A full description of the theory behind this technique has been published previously [21,22]. Briefly, V_{ATP} was calculated as the product of the pseudo-first-order rate constant for phosphate transfer from P_i to ATP (k_f) and the intramuscular concentration of P_i (Eq. 1). The rate constant k_f was calculated according to Eq. 2, where M_0 and M' represent the P_i signal during control and γ-ATP saturation conditions, respectively, and T_1' is the longitudinal relaxation time of P_i [21,22].

$$V_{ATP} = k_f [Pi] \quad \text{(Eq. 1)}$$

$$k_f = [1-M'/M_0] / T_1' \quad \text{(Eq. 2)}$$

General Procedure After an overnight fast, mice were placed prone on a plexiglass platform and anesthetized via a nose-cone with ~1% isoflurane in a 20:80 O_2:air mixture. Physiological parameters (body temperature, ECG, respiration rate) were monitored continuously to ensure the depth of anaesthesia and a heated water pad was used to maintain body temperature at ~37 °C. The mouse was positioned in an MR probe with the left hindlimb was secured under a 15 mm double-turn ^{31}P surface coil and within twin, orthogonal 25 mm diameter ^{1}H surface coils arrayed in quadrature. Mouse and probe were then placed in the isocenter of a 9.4 Tesla superconducting magnet (Magnex Scientific, Oxford, UK) interfaced to a Bruker Biospec console (Bruker BioSpin, Billerica, MA, USA). To maximize B_0 field homogeneity, the system was shimmed using the FASTMAP procedure.

Non-localized ^{31}P-MR spectra were acquired with frequency-selective saturation of the γ-ATP peak or with saturation at a downfield frequency equidistant from P_i (Fig. 3A), using the following parameters: 1ms adiabatic half passage (AHP excitation pulse centered between P_i and γ-ATP), 10s soft saturation pulse, sweep width = 8kHz, 1024 points, effective T_R = 10s, 64 transients. M'/M_0 was calculated by measuring the P_i peak integrals under γ-ATP and control symmetrical saturation. T_1' was measured for each animal using an 8-point

inversion-recovery sequence with γ-ATP saturation applied during the T_R and throughout inversion delay. Fully-relaxed ^{31}P spectra (T_R = 25s, 32 transients) without frequency-selective saturation were obtained to determine metabolite concentrations *in vivo*.

^{31}P FIDs were processed using XWINNMR version 6.5 (Bruker Biospin, Germany); FIDs were zero-filled to 32k points and multiplied by a mixed Lorentzian/Gaussian function (lb -20/ gb 0.04), prior to Fourier Transformation (FT). Spectra were manually phased (0 and 1st order) and baseline corrected by fitting the region of ^{31}P metabolites to a 5th order polynomial.

Ex vivo determination of ^{31}P metabolite concentrations in skeletal muscle Following the ^{31}P MR experiment, the skeletal muscles of each hindlimb were freeze-clamped *in situ* and extracted as reported elsewhere [23,24]. The lyophilized extracts were then re-suspended in 500 µl of buffer (20mM HEPES, 20mM EDTA, 0.5M KCl, 10% D_2O, pH ~5.5-6) containing 1mM phenylphosphonic acid (PPA) as an internal standard. Tissue ^{31}P-metabolite content of each extract was determined using high-resolution ^{31}P-NMR at 500MHz (Bruker Biospin, Billerica, MA). ^{31}P-Spectra were acquired with following parameters: 7.75µs square excitation pulse, sweep width = 50 ppm; 32k points; T_R = 1s; 8 dummy scans; 4096 transients, and analysed using XWINNMR. FIDs were apodized using a mixed lorentzian/gaussian function (lb = 2 / gb = 0.05) prior to FT, then zero / 1st order phased and baseline corrected. Absolute concentrations were calculated from the metabolite peak integral relative to that of the PPA standard, with appropriate corrections for T_1 relaxation determined from phantom calibrations.

Statistical Analysis: Values are presented as mean ± SEM except for the metabolic modelling (means ± SD). Statistical analyses were performed by using Graphpad Prism 5 software (San Diego, CA, USA). Data from matched WT and UCP3-TG mice were compared using an unpaired 2-tailed Student's t test. The precision of the metabolic modelling analysis was determined by performing 100 Monte-Carlo simulations of the raw data with the addition of random Gaussian noise within the CWave package to generate probability distributions for each modelled rate. Statistical significance was considered for $P<0.05$.

Study Approval: All procedures were approved by the Yale University Animal Care and Use Committee.

Results

Body composition and energy balance

UCP3-TG mice had significantly lower body fat and increased lean mass than WT mice fed the same, regular-chow diet (Table 1). On the day of the [2-^{13}C]-acetate infusion, UCP3-TG mice (n = 26) were 24.4 ± 0.69 g whereas WT mice (n = 16) were 26.5 ± 0.61 g ($P < 0.02$). These mice were 16-17 weeks old. On the day of the *in vivo* ^{31}P-MRS experiment, the body weights of the UCP3-TG mice were 24.9 ± 1.08 g whereas WT mice were 29.7 ± 0.99 g (n = 6 per group; $P < 0.01$). These latter mice were 15-16 weeks old. There was no body weight difference between group animals tested for V_{TCA} and V_{ATP}.

Locomotor activity was similar in both WT and UCP3-TG mice (Table 1). However, total energy expenditure and food intake were 20-30% higher in UCP3-TG than in age- and fat content-matched WT mice (Table 1). While resting oxygen consumption was significantly higher in UCP3-TG than in WT mice, there were no differences in the respiratory exchange ratio between the two groups (Table 1).

In vivo skeletal muscle TCA cycle flux (V_{TCA})

The appearance of [2-^{13}C]-acetate in plasma was identical between the UCP3-TG and WT groups (Figures 2A and 2E). Time courses of ^{13}C-label incorporation into muscle glutamate and glutamine are shown in Figure 2B - fitting of this data to a mathematical model of the TCA cycle was able to distinguish a significant increase in TCA cycle flux in UCP3-TG mice. Muscle concentrations of glutamate and glutamine were lower in the UCP3-TG with respect to WT mice (Figure 2D), and these differences were incorporated into the modelling analysis. Monte-Carlo analysis of the modelling data revealed a 38% increase in V_{TCA} in UCP3-TG mice relative to the control (0.1208 ± 0.0083 vs 0.0874 ± 0.0062 μmol/g/min, $P < 0.0005$, Figure 2C). There were no differences in V_{AC}/V_{TCA} (or V_{DIL}/V_{TCA}) between groups indicating an identical substrate preference (acetate vs pyruvate/free fatty acids) during these experiments (Table 2). For previous *in vivo* studies in human muscle (where [2-^{13}C]- or [3-^{13}C]-glutamate turnover cannot be reliably detected) the rate of αKG-glutamate exchange (V_X) was assumed

to be faster than the TCA cycle and non-limiting [25]. Interestingly, in this study, V_X was found to be comparable to V_{TCA} (Table 2), but this lower relative rate had no impact on the estimation of V_{TCA} (Supplemental Figure 2).

In vivo skeletal muscle $P_i \rightarrow ATP$ flux (V_{ATP})

We found no difference in the concentration of ATP – calculated from high resolution ^{31}P-NMR of hindlimb muscle extracts – between the UCP3-TG and WT groups (Table 3). Representative MR spectra acquired during the ^{31}P-saturation-transfer experiment are shown in Fig 3A. Muscle $P_i \rightarrow$ ATP flux is directly dependent on the unidirectional rate constant (k_f) for phosphate transfer from P_i to ATP and the P_i concentration [P_i]. Although not significant, there were trends for a lower k_f and decreased [P_i] in the UCP3-TG mice (Table 3). This resulted in a significant, 19% reduction in V_{ATP} in UCP3-TG versus WT mice (5.655 ± 0.272 vs 4.555 ± 0.290 μmol/g/min, P = 0.02, Fig. 3B). Additional parameters derived during the ^{31}P-saturation-transfer experiment (M'/M_0 and T_1') are shown in Table 3. The concentration of phosphocreatine (PCr), as well as the ratios of [PCr]/[ATP] and [ATP]/[ADP] – determined from the fully-relaxed *in-vivo* ^{31}P MR spectra – were not significantly different in UCP3-TG mice compared to their WT littermates (Table 3).

Mitochondrial Efficiency in UCP3-TG vs WT mice

Our data indicates that, under resting conditions, the overexpression of UCP3 resulted in a decrease in mitochondrial ATP production in muscle accompanied by an increase in substrate oxidation via the TCA cycle. Overall, this corresponds to a ~42% reduction in the efficiency of mitochondrial oxidative phosphorylation (64.7 WT vs 37.7 UCP3-TG, Fig. 4).

Discussion

The aim of these experiments was to study whether UCP3 modulates mitochondrial efficiency in mouse skeletal muscle *in vivo*. We used a combination of *in vivo* ^{31}P-MRS and isotopic labelling methods with *ex vivo* analysis to measure $P_i \rightarrow$ ATP flux (V_{ATP}) and the rate of substrate oxidation via the TCA cycle (V_{TCA}). We found that the overexpression of UCP3 in mice significantly increased V_{TCA} and decreased V_{ATP} in hindlimb skeletal muscle leading to a reduction in mitochondrial efficiency, measured as V_{ATP}/V_{TCA}.

The high homology of UCP3 with other proteins in the UCP superfamily [1] suggested that it may also uncouple mitochondrial oxidative phosphorylation. Since UCP3 is preferentially expressed in skeletal muscle [2], it could potentially play a crucial role in the regulation of energy balance both at the tissue and whole-body level [26–28].

Evidence supporting a role for UCP3 in energy balance comes primarily from whole-body studies conducted using the CLAMS metabolic cage system. Mice overexpressing UCP3 had significantly lower body weight than WT mice. The phenotype of the UCP3 transgenic mice is consistent with the higher energy expenditure observed in lower fat pads with respect to WT mice [16]. In our study, UCP3-TG mice had higher energy expenditure, lower body weight and lower body fat despite the higher food intake than controls.

Previously, Cadenas et al. suggested that increased metabolism and weight loss in overexpressing-UCP3 mice are the result of an overexpression artifact rather than an *in vivo* physiological uncoupling effect or a native activity of UCP3 [29]. Furthermore, uncoupling in mitochondria of mice overexpressing UCP3 was not inhibited by guanosine diphosphate (GDP), indicating that UCP3 was constitutively active. The same authors argued that UCP3 can catalyse an inducible proton conductance when activated by superoxide, therefore defending muscle mitochondria from reactive oxygen species (ROS). Superoxide, as a physiological activator of UCPs, increased proton conductance in rat skeletal muscle, which correlated with doubling of native UCP3 protein[14,30]. Yet, muscle-specific overexpression promoted muscle fatty acid oxidation (FAO), either in a complete or incomplete fashion, and protected mice from oxidative stress [31]. Choi et al. found that high-fat-fed UCP3-TG mice were protected against fat induced defects in insulin-stimulated muscle glucose metabolism

[16]. In fact, body fat-matched UCP3 mice showed normal whole body and muscle insulin sensitivity. Altogether these findings indicate that UCP3 may influence metabolic rate and the whole-body glucose homeostasis of the animals. Uncoupling slightly accelerates respiration and hence upstream metabolism, being beneficial for several physiological processes. In fact, UCP3 protein content in vastus lateralis muscle of middle-age individuals with type 2 diabetes was determined to be 50% of that in healthy subjects [6]. These UCP3 mice were hyperphagic but lean, and not obese, as shown elsewhere [32].

A more direct assessment of the UCP3 role in the regulation of energy metabolism comes from studies, in which, for example, weight reduction leads to a reduction in UCP3 mRNA expression and protein content along with reduction of resting metabolic rate [26,27].

It is interesting to note that skeletal muscle, which on demand undergoes extremely large increases in ATP utilization, expresses UCP3. We observed decreased rates of ATP phosphorylation as well as increased rates of mitochondrial oxidation in resting skeletal muscle in mice overexpressing UCP3 in muscle. UCP3 may allow rapid switching between proton leak and ATP synthesis in response to changes in ATP turnover and thus maintaining fluxes through metabolic pathways of substrate oxidation [33]. In our study, the decreased efficiency of muscle energy production caused a concomitant rise in basal TCA cycle flux and resting oxygen consumption. The increased rates of resting muscle TCA cycle flux may provide an advantage by permitting a more rapid response to an increased demand for ATP. UCP3 might therefore be playing an important role as energy regulator. Whether this is determined by specific modality of activation, either transport of fatty acid anions or ROS production, remains to be ascertained.

There has been a great deal of interest in UCP3 as a potential target for treating alterations of metabolism. In this perspective, it is being more and more encouraged as a long-term strategy that may involve increasing patients' metabolic rates by decreasing their metabolic efficiency. Obviously, it must be understood firstly how this protein is linked to the pathophysiology of several diseases, and whether UCP3-mediated mitochondrial dysfunctions lead to obesity, diabetes, ages-related changes et cetera.

In the past, some methods for ATP assays erroneously show major non-physiological differences in cellular and tissue ATP concentrations. Here we used *in vivo* MRS to assess muscle mitochondrial coupling.

The flux through the tricarboxylic acid cycle may be used as an index of oxygen consumption under resting conditions. Consistently with earlier studies, an increased overexpression of UCP3 was associated with uncoupling activity under certain conditions, like T3 treatment [34] or fasting [35]. To date, only a few studies have assessed *in vivo* energy mitochondrial coupling using MRS [11,34,35]. Cline et al. achieved a 2-4 fold higher coupling of oxidative phosphorylation in mice lacking UCP3 [11], only relying on the increased TCA cycle flux.

These data are consistent with UCP3 mediating the uncoupling of oxidative phosphorylation *in vivo*. We have demonstrated that combining *in vivo* ^{31}P-MRS to determine $P_i \rightarrow$ ATP flux with an *ex-vivo,* serial biopsy, method to estimate TCA cycle flux from ^{13}C-labelled glutamate turnover allowed us to effectively assess muscle mitochondrial function in mice. Muscle specific rates of unidirectional $P_i \rightarrow$ ATP flux were 19% lower and muscle specific rates of TCA cycle flux were increased by 38% in UCP3-TG compared to WT mice. Together, these indices of mitochondrial function indicate that UCP3-TG mice exhibit reduced efficiency of muscle mitochondrial oxidative phosphorylation by approximately 42%. This study supports the hypothesis that UCP3 may function as a true uncoupler of mitochondrial oxidative phosphorylation *in vivo*. Further studies are necessary for exploring the regulation of uncoupling protein activity in mice, either within a physiological or pathophysiological context.

Author Contributions R.C., T.A., D.B. and G.I.S., designed the experiments. R.C., T.A. and D.B performed the experiments. All authors analyzed data and contributed to writing the manuscript. G.S. is the guarantor of this work and, as such, had full access to all the data in the study and takes responsibility for the integrity of data and the accuracy of data analysis.

Acknowledgements This work was supported by a grant from European Commission (FP7-PEOPLE-2009-RG, project "INMARESS", n° 256506) and by NIH grants: R01 DK40936, R01 DK108283, P30 DK45735, U24 DK59635, U24 DK76169 and P30 NS52519.

Conflict of Interest The authors have declared that no conflict of interest exists.

Data availability The data supporting the findings of this study are available on request from the authors.

References

1 Andrews ZB, Diano S & Horvath TL (2005) Mitochondrial uncoupling proteins in the CNS: in support of function and survival. *Nat Rev Neurosci* **6**, 829–40.

2 Vidal-Puig A, Solanes G, Grujic D, Flier JS & Lowell BB (1997) UCP3: An Uncoupling Protein Homologue Expressed Preferentially and Abundantly in Skeletal Muscle and Brown Adipose Tissue. *Biochem Biophys Res Commun* **235**, 79–82.

3 Boss O, Samec S, Paoloni-Giacobino A, Rossier C, Dulloo A, Seydoux J, Muzzin P & Giacobino JP (1997) Uncoupling protein-3: a new member of the mitochondrial carrier family with tissue-specific expression. *FEBS Lett* **408**, 39–42.

4 Matsuda J, Hosoda K, Itoh H, Son C, Doi K, Tanaka T, Fukunaga Y, Inoue G, Nishimura H, Yoshimasa Y, Yamori Y & Nakao K (1997) Cloning of rat uncoupling protein-3 and uncoupling protein-2 cDNAs: their gene expression in rats fed high-fat diet. *FEBS Lett* **418**, 200–4.

5 Gong DW, He Y, Karas M & Reitman M (1997) Uncoupling protein-3 is a mediator of thermogenesis regulated by thyroid hormone, beta3-adrenergic agonists, and leptin. *J Biol Chem* **272**, 24129–32.

6 Schrauwen P, Hesselink MK, Blaak EE, Borghouts LB, Schaart G, Saris WH & Keizer HA (2001)

Uncoupling protein 3 content is decreased in skeletal muscle of patients with type 2 diabetes. *Diabetes* **50**, 2870–3.

7 Andrews ZB (2010) Uncoupling protein-2 and the potential link between metabolism and longevity. *Curr Aging Sci* **3**, 102–12.

8 Speakman JR, Talbot DA, Selman C, Snart S, McLaren JS, Redman P, Krol E, Jackson DM, Johnson MS & Brand MD (2004) Uncoupled and surviving: individual mice with high metabolism have greater mitochondrial uncoupling and live longer. *Aging Cell* **3**, 87–95.

9 Clapham JC, Arch JR, Chapman H, Haynes A, Lister C, Moore GB, Piercy V, Carter SA, Lehner I, Smith SA, Beeley LJ, Godden RJ, Herrity N, Skehel M, Changani KK, Hockings PD, Reid DG, Squires SM, Hatcher J, Trail B, Latcham J, Rastan S, Harper AJ, Cadenas S, Buckingham JA, Brand MD & Abuin A (2000) Mice overexpressing human uncoupling protein-3 in skeletal muscle are hyperphagic and lean. *Nature* **406**, 415–8.

10 Vidal-Puig AJ, Grujic D, Zhang CY, Hagen T, Boss O, Ido Y, Szczepanik A, Wade J, Mootha V, Cortright R, Muoio DM & Lowell BB (2000) Energy metabolism in uncoupling protein 3 gene knockout mice. *J Biol Chem* **275**, 16258–66.

11 Cline GW, Vidal-Puig AJ, Dufour S, Cadman KS, Lowell BB & Shulman GI (2001) In vivo effects of uncoupling protein-3 gene disruption on mitochondrial energy metabolism. *J Biol Chem* **276**, 20240–4.

12 Barger JL, Barnes BM & Boyer BB (2006) Regulation of UCP1 and UCP3 in arctic ground squirrels and relation with mitochondrial proton leak. *J Appl Physiol* **101**, 339–347.

13 Cline GW (2006) Tough love: left out in the cold, but not abandoned, by UCP3. *J Appl Physiol* **101**, 12–3.

14 Echtay KS, Esteves TC, Pakay JL, Jekabsons MB, Lambert AJ, Portero-Otín M, Pamplona R, Vidal-Puig AJ, Wang S, Roebuck SJ & Brand MD (2003) A signalling role for 4-hydroxy-2-nonenal in regulation of mitochondrial uncoupling. *EMBO J* **22**, 4103–10.

15 Choi CS, Befroy DE, Codella R, Kim S, Reznick RM, Hwang Y-J, Liu Z-X, Lee H-Y, Distefano A, Samuel VT, Zhang D, Cline GW, Handschin C, Lin J, Petersen KF, Spiegelman BM & Shulman GI (2008) Paradoxical effects of increased expression of PGC-1 on muscle mitochondrial function and insulin-

stimulated muscle glucose metabolism. *Proc Natl Acad Sci* **105**, 19926–19931.

16 Choi CS, Fillmore JJ, Kim JK, Liu Z-X, Kim S, Collier EF, Kulkarni A, Distefano A, Hwang Y-J, Kahn M, Chen Y, Yu C, Moore IK, Reznick RM, Higashimori T & Shulman GI (2007) Overexpression of uncoupling protein 3 in skeletal muscle protects against fat-induced insulin resistance. *J Clin Invest* **117**, 1995–2003.

17 Powers L, Osborne MK, Yang D, Kien CL, Murray RD, Beylot M & Brunengraber H (1995) Assay of the concentration and stable isotope enrichment of short-chain fatty acids by gas chromatography/mass spectrometry. *J Mass Spectrom* **30**, 747–754.

18 de Graaf RA (2007) *In Vivo NMR Spectroscopy: Principles and Techniques: 2nd Edition*.

19 Alves TC, Befroy DE, Kibbey RG, Kahn M, Codella R, Carvalho RA, Petersen KF, Shulman GI, Falk Petersen K & Shulman GI (2011) Regulation of hepatic fat and glucose oxidation in rats with lipid-induced hepatic insulin resistance. *Hepatology* **53**, 1175–81.

20 Mason GF, Falk Petersen K, de Graaf RA, Kanamatsu T, Otsuki T, Shulman GI & Rothman DL (2003) A comparison of (13)C NMR measurements of the rates of glutamine synthesis and the tricarboxylic acid cycle during oral and intravenous administration of [1-(13)C]glucose. *Brain Res Brain Res Protoc* **10**, 181–90.

21 Forsén S, Hoffman RA, Hirvisalo EL, Munch-Petersen J & Munch-Petersen J (1963) A New Method for the Study of Moderately Rapid Chemical Exchange Rates Employing Nuclear Magnetic Double Resonance. *Acta Chem Scand* **17**, 1787–1788.

22 Forsén S & Hoffman RA (1963) Study of Moderately Rapid Chemical Exchange Reactions by Means of Nuclear Magnetic Double Resonance. *J Chem Phys* **39**, 2892–2901.

23 Le Belle JE, Harris NG, Williams SR & Bhakoo KK (2002) A comparison of cell and tissue extraction techniques using high-resolution 1H-NMR spectroscopy. *NMR Biomed* **15**, 37–44.

24 Wu H, Southam AD, Hines A & Viant MR (2008) High-throughput tissue extraction protocol for NMR- and MS-based metabolomics. *Anal Biochem* **372**, 204–12.

25 Befroy DE, Falk Petersen K, Rothman DL & Shulman GI (2009) Assessment of in vivo mitochondrial

metabolism by magnetic resonance spectroscopy. *Methods Enzymol* **457**, 373–93.

26 Schrauwen P, Schaart G, Saris WHM, Slieker LJ, Glatz JFC, Vidal H & Blaak EE (2000) The effect of weight reduction on skeletal muscle UCP2 and UCP3 mRNA expression and UCP3 protein content in Type II diabetic subjects. *Diabetologia* **43**, 1408–1416.

27 Vidal H, Langin D, Andreelli F, Millet L, Larrouy D & Laville M (1999) Lack of skeletal muscle uncoupling protein 2 and 3 mRNA induction during fasting in type-2 diabetic subjects. *Am J Physiol* **277**, E830-7.

28 Schrauwen P, Xia J, Bogardus C, Pratley RE & Ravussin E (1999) Skeletal muscle uncoupling protein 3 expression is a determinant of energy expenditure in Pima Indians. *Diabetes* **48**, 146–9.

29 Cadenas S, Echtay KS, Harper JA, Jekabsons MB, Buckingham JA, Grau E, Abuin A, Chapman H, Clapham JC & Brand MD (2002) The basal proton conductance of skeletal muscle mitochondria from transgenic mice overexpressing or lacking uncoupling protein-3. *J Biol Chem* **277**, 2773–2778.

30 Echtay KS, Roussel D, St-Plerre J, Jekabsons MB, Cadenas S, Stuart JA, Harper JA, Roebuck SJ, Morrison A, Pickering S, Clapham JC & Brand MD (2002) Superoxide activates mitochondrial uncoupling proteins. *Nature* **415**, 96–99.

31 Aguer C, Fiehn O, Seifert EL, Bezaire V, Meissen JK, Daniels A, Scott K, Renaud J-M, Padilla M, Bickel DR, Dysart M, Adams SH & Harper M-E (2013) Muscle uncoupling protein 3 overexpression mimics endurance training and reduces circulating biomarkers of incomplete -oxidation. *FASEB J* **27**, 4213–4225.

32 Choi CS, Savage DB, Abu-Elheiga L, Liu Z-XZ-X, Kim S, Kulkarni A, Distefano A, Hwang Y-J, Reznick RM, Codella R, Zhang D, Cline GW, Wakil SJ & Shulman GI (2007) Continuous fat oxidation in acetyl-CoA carboxylase 2 knockout mice increases total energy expenditure, reduces fat mass, and improves insulin sensitivity. *Proc Natl Acad Sci U S A* **104**, 16480–16485.

33 Kelley DE (2005) Skeletal muscle fat oxidation: timing and flexibility are everything. *J Clin Invest* **115**, 1699–1702.

34 Jucker BM, Dufour S, Ren J, Cao X, Previs SF, Underhill B, Cadman KS & Shulman GI (2000) Assessment of mitochondrial energy coupling in vivo by 13C/31P NMR. *Proc Natl Acad Sci U S A* **97**, 6880–4.

35 Jucker BM, Ren J, Dufour S, Cao X, Previs SF, Cadman KS & Shulman GI (2000) 13C/31P NMR

assessment of mitochondrial energy coupling in skeletal muscle of awake fed and fasted rats. Relationship with uncoupling protein 3 expression. *J Biol Chem* **275**, 39279–86.

Tables

Table 1. Body composition and energy balance data WT and UCP3-TG mice fed regular chow.

Table 2. Muscle metabolic fluxes obtained from CWave simulation and Monte-Carlo analysis of ^{13}C-labelled glutamate and glutamine turnover during an infusion of [2-^{13}C]-acetate. Data is shown as the least-square fit ± standard deviation of the distribution obtained from the Monte-Carlo simulations.

Table 3. Phosphate metabolite concentrations, $P_i \rightarrow ATP$ flux and ^{31}P saturation-transfer parameters NMR-obtained (500MHz) from the hind-limb muscles of WT and UCP3-TG mice.

Figure legends

Figure 1. ***Estimating skeletal muscle TCA cycle flux (V_{TCA}) using a serial biopsy-based technique***

(**A**) Experimental protocol for the serial biopsy procedure. Animals were anesthetized using 1% isoflurane in air/O_2 delivered via nose-cone; physiological parameters were continuously monitored. Following a 60min stabilization period, [2-^{13}C]-acetate was infused (10.2 μg/g/min) via a jugular vein catheter. Plasma samples were obtained by tail-tip bleed at regular intervals throughout the infusion (black arrows). Grey arrows indicate the times at which hindlimb skeletal muscle tissue was excised. (**B**) Metabolic model describing the entry of plasma [2-^{13}C]acetate into the TCA cycle and ^{13}C-label flow during consecutive turns of the cycle in the skeletal muscle. The C_X prefix before each metabolite denotes the position of ^{13}C-labelling during the infusion experiment. AcCoA = acetyl CoA; αKG = alpha-ketoglutarate; OAA = oxaloacetate. V_{TCA} = TCA cycle flux; V_{AC} = rate of acetate entry into the acetyl CoA pool; V_{DIL} = rate of entry of unlabelled precursors (pyruvate, free fatty acids) into the acetyl CoA pool; V_X = rate of αKG-glutamate exchange; V_{GS} = rate of glutamate-glutamine exchange; $V_{Dil\text{-}Gln}$ = dilution of the glutamine pool.

Figure 2. (**A**) Time courses of [2-^{13}C]-acetate enrichment for WT and UCP3 TG mice. (**B**) Muscle [4-^{13}C]-, [3-^{13}C]-glutamate and [4-^{13}C]-glutamine enrichments during the [2-^{13}C]-acetate infusion for the WT and UCP3-TG groups; fits of the enrichment data modelled using CWave are superimposed. (**C**) Estimates of muscle V_{TCA} obtained from the metabolic modelling analysis. (**D**) Concentrations of glutamate, glutamine and acetate in the muscle of wild type and UCP3-TG mice. (**E**) Time courses of plasma acetate concentrations. In (**C**) data are shown as least-square fit ± standard deviation of the distribution obtained from the Monte-Carlo distributions.

Figure 3. ***In vivo skeletal muscle $P_i \rightarrow ATP$ flux (V_{ATP}) determined using ^{31}P-saturation-transfer MRS***

(**A**) Representative ^{31}P-MR spectra acquired during a saturation transfer experiment. Frequency-selective saturation of the γ-ATP peak (red spectrum) leads to a reduction in the magnitude of the P_i peak (at ~5.1ppm) due to $P_i \rightarrow$ ATP flux. The control spectrum (in blue) is acquired with the saturation pulse applied at a frequency downfield of P_i equidistant from γ-ATP. The difference between the magnitude of the P_i peak (ΔP_i) is proportional to the rate constant for unidirectional $P_i \rightarrow$ ATP flux (k_f); $V_{ATP} = k_f \cdot [P_i]$. (**B**) V_{ATP} in wild type (WT) and transgenic mice (UCP3-TG). Data are expressed as mean ± SEM.

Figure 4. The efficiency of muscle mitochondrial oxidative phosphorylation in WT and UCP3-TG mice estimated as the ratio of Pi → ATP flux over TCA cycle flux. Data are expressed as mean ± SD.

Table 1. Body composition and energy balance data WT and UCP3-TG mice fed regular chow.

	WT	UCP3-TG	p-value
Fat mass (% body mass)	16.1 ± 1.2	12.8 ± 0.7	< 0.05
Lean mass (% body mass)	68.1 ± 1.5	72.9 ± 1.7	< 0.05
RER (respiratory exchange ratio)	0.91 ± 0.01	0.92 ± 0.02	0.33
Energy Expenditure (kcal/kg/h)	18.7 ± 0.4	24.0 ± 0.6	< 0.001
VO_2 (l/kg/h)	3781.3 ± 73.8	4895.2 ± 93.5	< 0.001
Food Intake (g/kg/h)	1.2 ± 0.1	1.8 ± 0.1	0.016
Locomotor Activity (count/h)	101.0 ±14.7	101.9 ± 17.7	0.96

Data are expressed as mean ± SEM.

Table 2. Muscle metabolic fluxes obtained from CWave simulation and Monte-Carlo analysis of ^{13}C-labelled glutamate and glutamine turnover during an infusion of [2-^{13}C]-acetate. Data is shown as the least-square fit ± standard deviation of the distribution obtained from the Monte-Carlo simulations.

	WT (n = 16)	UCP3-TG (n = 26)
V_{TCA} (µmol/g/min)	0.0874 ± 0.0062	0.1208 ± 0.0083 **
V_{AC} (µmol/g/min)	0.0818 ± 0.0055	0.1114 ± 0.0083 *
V_{DIL} (µmol/g/min)	0.0056 ± 0.0092	0.0094 ± 0.0115
V_{AC}/V_{TCA}	0.94 ± 0.09	0.92 ± 0.09
V_{DIL}/V_{TCA}	0.06 ± 0.09	0.08 ± 0.09
V_{GS} (µmol/g/min)	0.0526 ± 0.0055	0.1044 ± 0.0101 **
$V_{DIL\text{-}Gln}$ (µmol/g/min)	0.1535 ± 0.0186	0.2457 ± 0.0253 *
V_X (µmol/g/min)	0.0825 ± 0.0277	0.1471 ± 0.0484

* P < 0.005, ** P < 0.0005

Data are expressed as mean ± SD

Table 3. Phosphate metabolite concentrations, $P_i \rightarrow ATP$ flux and ^{31}P saturation-transfer parameters NMR-obtained (500MHz) from the hind-limb muscles of WT and UCP3-TG mice.

	WT (n = 6)	UCP3-TG (n = 6)	p-value

[ATP] ($\mu mol.g^{-1}$)	3.36 ± 0.34	3.41 ± 0.53	0.93
[P_i] ($\mu mol.g^{-1}$)	1.37 ± 0.07	1.30 ± 0.07	0.48
[PCr] ($\mu mol.g^{-1}$)	9.25 ± 0.87	9.98 ± 0.49	0.48
[γ-ATP] / [β-ADP]	5.73 ± 0.13	5.84 ± 0.21	0.69
[PCr] / [γ-ATP]	2.75 ± 0.26	2.92 ± 0.07	0.58
k_f (sec^{-1})	0.069 ± 0.01	0.060 ± 0.01	0.21
M'/ M_0	0.768 ± 0.02	0.771 ± 0.01	0.88
$T_1'(P_i)$ (sec)	3.34 ± 0.14	3.94 ± 0.26	0.08
V_{ATP} (μmol/g/min)	5.655 ± 0.272	4.555 ± 0.290	0.02

Data are expressed as mean ± SEM.

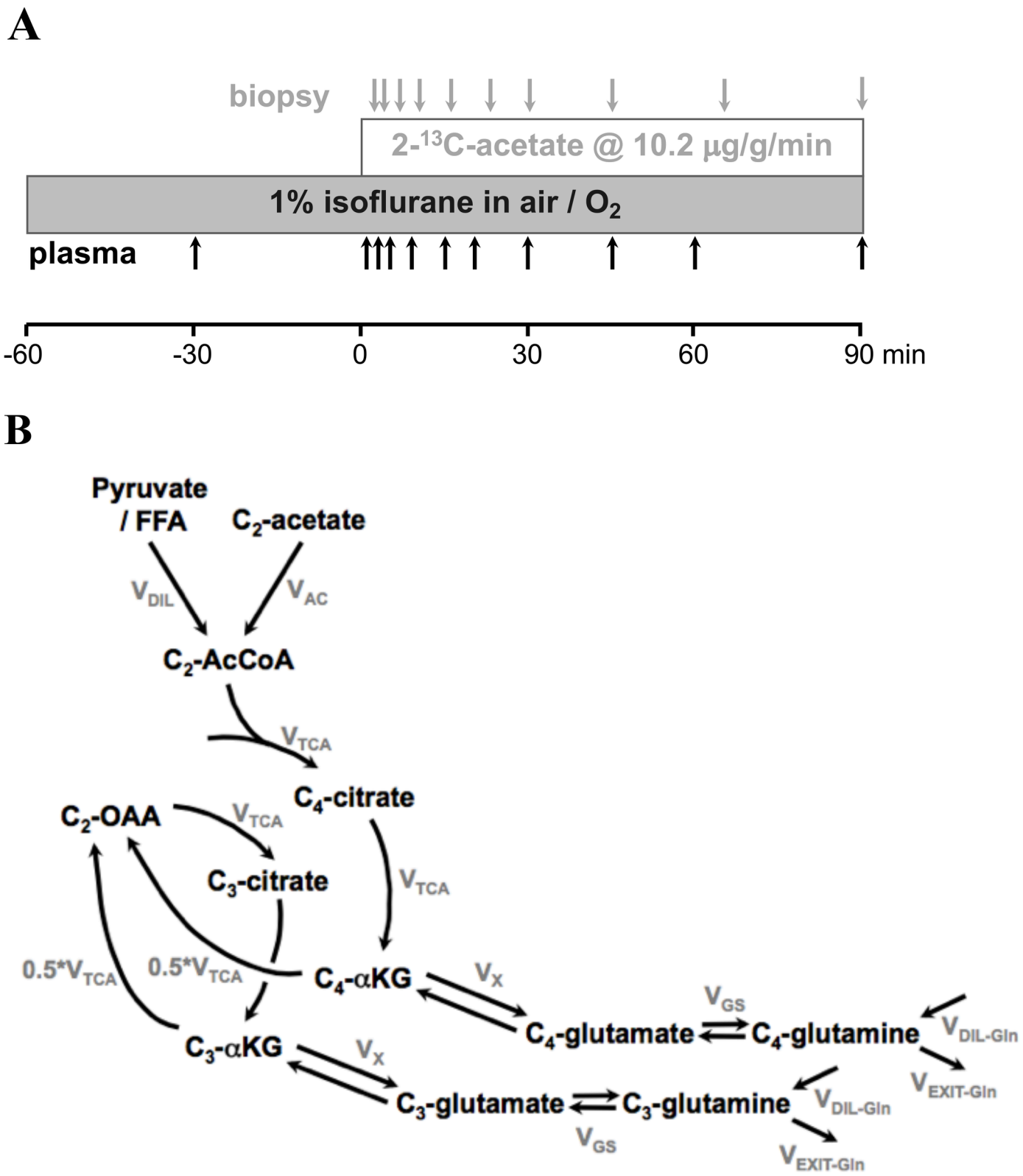

FEB2_14494_Figure 1_FEBS.tif

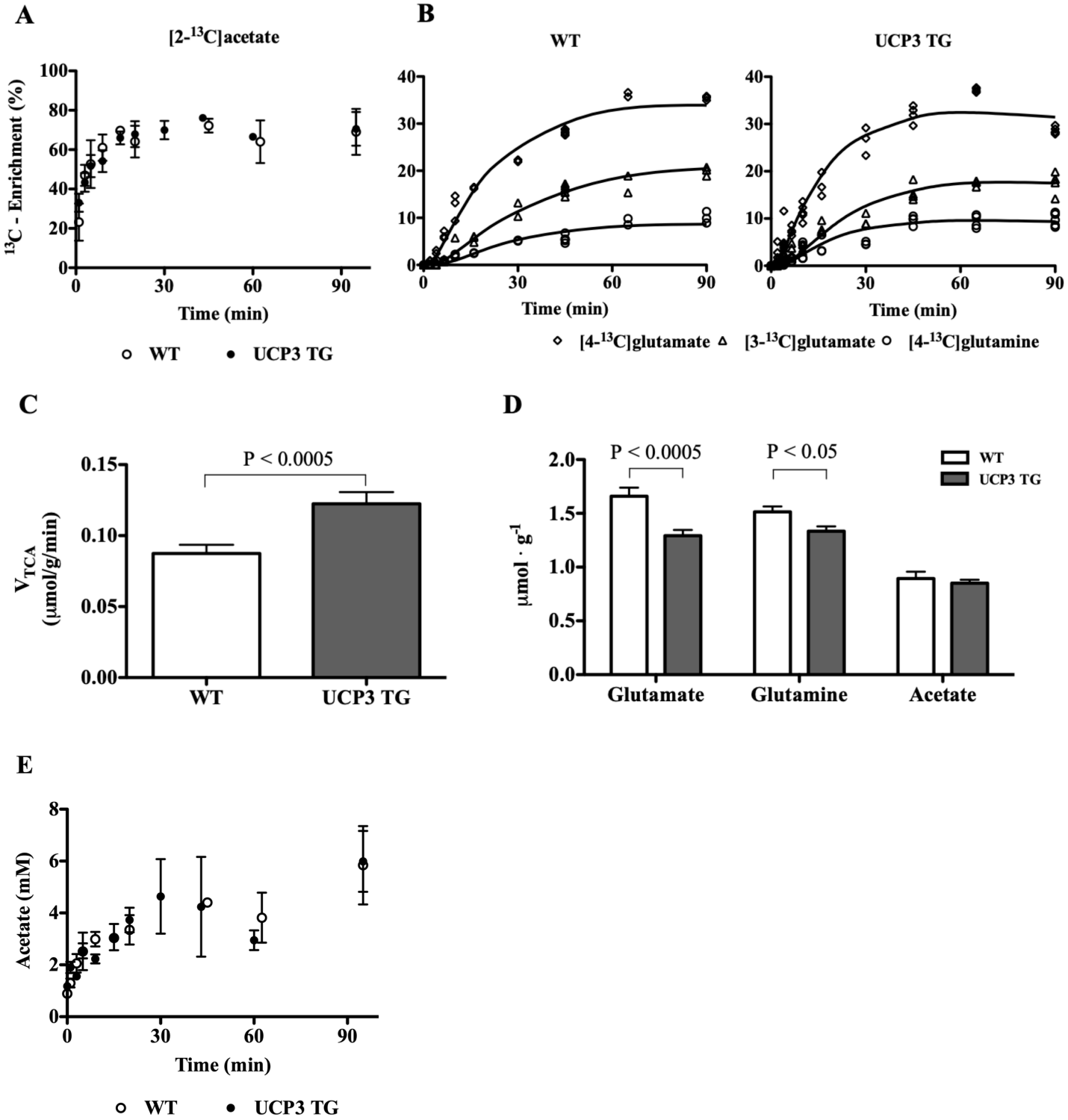

FEB2_14494_Figure_2_FEBS.tif

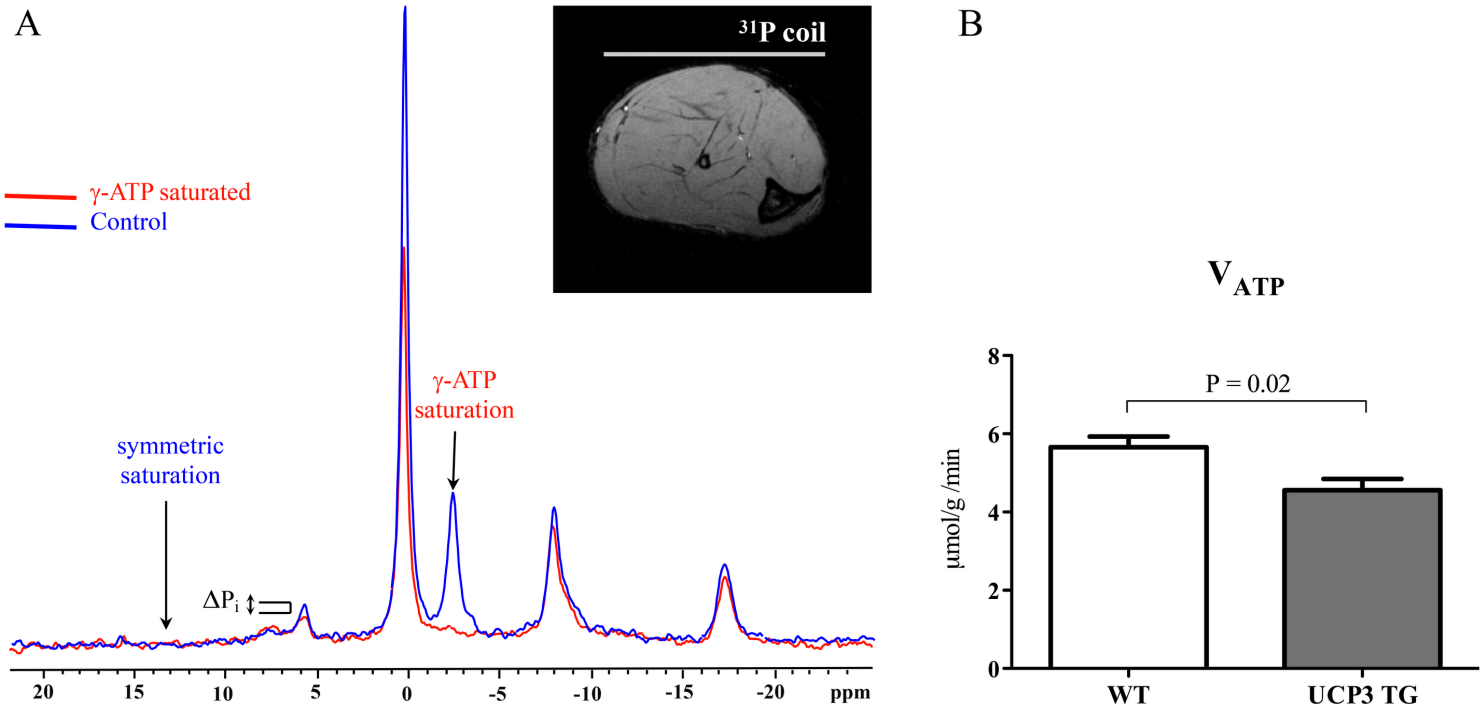

FEB2_14494_Figure 3_FEBS_0563.R1.tif

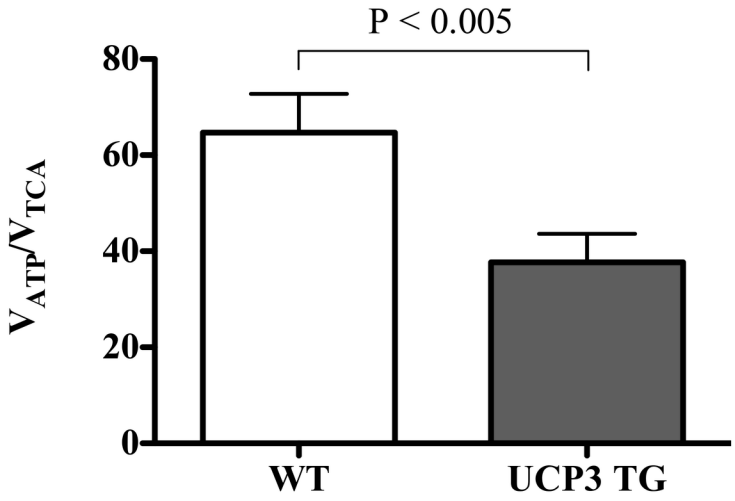

FEB2_14494_Figure 4_FEBS.tif